Metal Binding of Polyalcohols. 4.† Structure and Magnetism of the Hexanuclear, μ_6-Oxo-Centered $[OFe_6(H_{-3}thme)_3(OCH_3)_3Cl_6]^{2-}$ (thme = 1,1,1-Tris(hydroxymethyl)ethane)

Andrea Cornia

Dipartimento di Chimica, Università di Modena, 41100 Modena, Italy

Dante Gatteschi

Dipartimento di Chimica, Università di Firenze, 50144 Florence, Italy

Kaspar Hegetschweiler*

Institut für Anorganische Chemie, Universität des Saarlandes, Postfach 15 11 50, D-66041 Saarbrücken, Germany

Lorenza Hausherr-Primo

Laboratorium für Anorganische Chemie, ETH Zentrum, CH-8092 Zürich, Switzerland

Volker Gramlich

Institut für Kristallographie, ETH Zentrum, CH-8092 Zürich, Switzerland

Received January 10, 1996⊗

The addition of $[N(CH_3)_4]OH$ to a methanolic solution of $FeCl_3$ and thme (thme = 1,1,1-tris(hydroxymethyl)-ethane) yielded $[N(CH_3)_4]_2[OFe_6(H_{-3}thme)_3(OCH_3)_3Cl_6]\cdot 2H_2O$ (**1**). Crystal data: $C_{26}H_{64}Cl_6Fe_6N_2O_{15}$, trigonal space group $P31c$, $a = 12.459(2)$ Å, $c = 18.077(4)$ Å, $Z = 2$. The complex anion exhibits the well-known μ_6-O−Fe_6−$(\mu_2$-$OR)_{12}$ structure with three μ_2-methoxo bridges, three triply deprotonated H_{-3}thme ligands, where each alkoxo group bridges two Fe^{III} centers, and six terminally coordinating Cl^- ligands. In contrast to two previously described ferric complexes with an analogous structure of the complex core, compound **1** is stable in air. Variable-temperature magnetic susceptibility measurements established antiferromagnetic exchange coupling interactions with J_{trans}(Fe−μ_6-O−Fe) = 24.5 cm^{-1}, J_{cis}(Fe−μ_2-O_{thme}−Fe) = 11.5 cm^{-1}, and J_{cis}'(Fe−μ_2-OCH_3−Fe) = 19.5 cm^{-1}. The unexpectedly high value for J_{trans} is explained by means of a superexchange pathway and is discussed for a simplified model by using MO calculations at the extended Hückel level.

Introduction

The synthesis and structural characterization of metal alkoxo complexes has received considerable attention lately since these compounds have been successfully used as precursors for the preparation of new materials by MOCVD and sol−gel techniques.[1] Although polyalcohols are among the most abundant biological materials, it has not widely been recognized that they could serve as a promising pool of new, interesting multidentate ligands providing a large variety of specific metal binding sites.[2] In the presence of water, the hydrolytic polymerization, leading to solid oxides or hydroxides, and the formation of soluble alkoxo complexes are competitive and also the combination of the two reactions, i.e. the formation of polynuclear alkoxo−oxo or alkoxo−hydroxo complexes, can occur. As an example, we recently studied the hydrolytic polymerization of $FeCl_3$ in the presence of either *cis*-inositol or 1,1,1-tris(hydroxymethyl)-ethane (thme).[3,4] Both reactions resulted in the formation of a hexanuclear complex, containing a bridging oxygen atom in the center and six polyolato ligands at the periphery, which shield the complex core effectively and prevent further aggregation. Bridging and terminal alkoxo groups are present in both complexes, and the coordination of the polyols occurred exclusively under deprotonation. However, in the *cis*-inositol complex only three of the six ferric ions are bound to the central oxygen atom and the complex did not show any point symmetry, whereas in the thme complex all six ferric ions are bound to the central oxygen atom resulting in a complex with approximate S_6 symmetry. Moreover, in the *cis*-inositol complex, every ligand molecule interacts in a different way with the metal centers, whereas the thme ligands all show the same type of coordination. It would thus be of considerable interest to

* Author to whom correspondence should be addressed.

† For part 3, see ref 3.

⊗ Abstract published in *Advance ACS Abstracts,* June 1, 1996.

(1) Hubert-Pfalzgraf, L. G. *New J. Chem.* **1987**, *11*, 663. Brinker, C. J.; Scherer, G. W. *Sol-gel science: the physics and chemistry of sol-gel processing*; Academic Press: San Diego, CA, 1990. Caneschi, A.; Cornia, A.; Fabretti, A. C.; Gatteschi, D.; Malavasi, W. *Inorg. Chem.* **1995**, *34*, 4660. Caneschi, A.; Cornia, A.; Lippard, S. J. *Angew. Chem.* **1995**, *107*, 511; *Angew. Chem., Int. Ed. Engl.* **1995**, *34*, 467. Caneschi, A.; Cornia, A.; Fabretti, A. C.; Gatteschi, D. *Angew. Chem.* **1995**, *107*, 2862; *Angew. Chem., Int. Ed. Engl.* **1995**, *34*, 2716.

(2) Burger, J.; Gack, C.; Klüfers, P. *Angew. Chem., Int. Ed. Engl.* **1995**, *34*, 2647.

(3) Hegetschweiler, K.; Hausherr-Primo, L.; Koppenol, W. H.; Gramlich, V.; Odier, L.; Meyer, W.; Winkler, H.; Trautwein, A. X. *Angew. Chem.* **1995**, *107*, 2421; *Angew. Chem., Int. Ed. Engl.* **1995**, *34*, 2242.

(4) Hegetschweiler, K.; Schmalle, H.; Streit, H. M.; Schneider, W. *Inorg. Chem.* **1990**, *29*, 3625.

S0020-1669(96)00025-0 CCC: $12.00

Table 1. Crystallographic Data for $[N(CH_3)_4]_2[OFe_6(H_{-3}thme)_3(OCH_3)_3Cl_6]\cdot 2H_2O$ (**1**)

chem formula	$C_{26}H_{64}Cl_6Fe_6N_2O_{15}$
fw	1192.60
space group	*P*31*c* (No. 159)
a	12.459(2) Å
c	18.077(4) Å
V	2430.1(8) Å^3
Z	2
T	20 °C
λ	0.710 73 Å
ρ_{calcd}	1.63 g cm^{-3}
μ(Mo Kα)	21.4 cm^{-1}
$R(F_o)^a$	0.061
$R_w(F_o)^b$	0.063

[a] $R = \sum(||F_o| - |F_c||)/\sum|F_o|$. [b] $R_w = [(||F_o| - |F_c||)^2/\sum w|F_o|^2]^{1/2}$, $w^{-1} = \sigma^2(F_o) + 0.0007F_o^2$.

understand more precisely how a specific steric arrangement of hydroxy groups influences the structure of the corresponding cluster core. In the present study, we have investigated the Fe^{III}−thme interaction under different reaction conditions and established a second coordination mode of the deprotonated H_{-3}thme ligand. In addition, a comprehensive analysis of the magnetic properties of the resulting complex has been performed.

Experimental Section

Materials and Analyses. $FeCl_3$ (anhydrous), 1,1,1-tris(hydroxymethyl)ethane (thme), $[N(CH_3)_4]OH$, diethyl ether, and MeOH were commercially available compounds (from Fluka, Switzerland) and were used without further purification. C, H, and N analyses were performed by D. Manser, Laboratorium für Organische Chemie, ETH-Zürich.

Synthetic Work. A solution (1.5 mL) of $FeCl_3$ (2 mmol) in MeOH was added to a methanolic solution (1 mL) of thme (2 mmol). The resulting clear, orange solution was diluted with MeOH to a total volume of 10 mL. $[N(CH_3)_4]OH$ (6 mmol), dissolved in MeOH (6 mL), was added slowly with stirring. A brown solid precipitated almost quantitatively. The suspension was allowed to stay in the dark for 1 d at ambient temperature, and a brown solid having the tentative composition $[N(CH_3)_4]_2[OFe_6(H_{-3}thme)_3(OCH_3)_3Cl_6]\cdot$MeOH was filtered off. Anal. Calc for $C_{27}H_{64}Cl_6Fe_6N_2O_{14}$: C, 27.28; H, 5.43; N, 2.36. Found: C, 27.20; H, 5.50; N, 2.15. The solid was ground up and redissolved in MeOH. Single crystals of $[N(CH_3)_4]_2[OFe_6(H_{-3}thme)_3(OCH_3)_3Cl_6]\cdot 2H_2O$ (**1**) were grown by layering the resulting brown solution with diethyl ether. The crystals (yield: 20%) proved to be air stable and were suitable for X-ray analysis. Anal. Calc for $C_{26}H_{64}Cl_6Fe_6N_2O_{15}$: C, 26.19; H, 5.41; N, 2.35. Found: C, 26.28; H, 5.46; N, 2.33.

Single-Crystal X-ray Diffraction Studies. A reddish brown crystal of **1** was mounted on a Syntex P21 four-circle diffractometer. Graphite-monochromatized Mo Kα radiation was used for data collection (Table 1). No significant decay of the crystal was noted during the measurement; however, due to the small dimensions of the crystal (0.05 × 0.05 × 0.1 mm) only a limited amount of data (4700 reflections, 3° < 2θ < 40°) could be collected. A total of 554 of the 794 unique reflections ($R_{int} = 0.037$) were considered observed with $I > 2\sigma(I)$. A face-indexed, numerical absorption correction was applied (min and max transmission coefficients were 0.7465 and 0.7592), and the data were corrected for Lorentz and polarization effects. The structure was solved by the Patterson method of SHELXTL PLUS (VMS)[5] and refined by full-matrix least-squares calculations. Inspection of the packing (e.g. along *c*) clearly confirmed the presence of a noncentrosymmetric space group: one type of the triad axes of the trigonal space group is occupied by the noncentrosymmetrical iron complex, and the other, nonequivalent one, by the tetrahedral counterion. The C(6) position (methoxo ligands) was poorly localizable and appeared only after several refinement cycles. In addition, two oxygen positions corresponding to four water molecules per complex were located. However, the rather large displacement parameters indicated a crystallographic disorder of the two water positions and a refinement of the occupancy factors clearly showed that O(1w) and O(2w) are only partially occupied. In agreement with the elemental analysis which requires a total of two water molecules of crystallization, fixed occupancy factors of 0.5 were used for both positions in the subsequent refinement. All non-hydrogen atoms could be refined successfully in the anisotropic mode giving an *R*-factor of 5.68% (R_w = 5.77%). However, the low data to parameter ratio of 3.7 was not acceptable. Therefore, the refinement was repeated by treating the $N(CH_3)_4$ counterions as fixed models with N−C distances of 1.50 Å. The carbon−carbon distances in the ligand were constrained to a value of 1.547 Å. H(−C) positions where then calculated, and the carbon−hydrogen skeleton was refined as a rigid body with a fixed C−C−C angle of 109.5°. By this way, a more satisfying data to parameter ratio of 5.5 (101 parameters) was obtained. The *R*-factor increased slightly to a value of 6.06%. In order to obtain an optimal fit the structure was also refined with inverse coordinates. However, no significant difference was noted (the *R*-factor increased by 0.002). This result is not unexpected since the space group *P*31*c* is noncentrosymmetric but not chiral. The final atomic coordinates are shown in Table 2.

Table 2. Atomic Coordinates and Isotropic or Equivalent Isotropic Displacement Parameters for Non-Hydrogen Atoms of **1** with Esd's in Parentheses

atom	*x*	*y*	*z*	U_{eq}/U_{iso},[a] Å^2
Fe(1)	0.1989(3)	0.5078(3)	0.5682	0.040(2)
Fe(2)	0.1767(4)	0.6457(3)	0.7123(2)	0.047(3)
Cl(1)	0.0612(8)	0.3458(7)	0.4946(5)	0.062(5)
Cl(2)	0.0179(9)	0.6284(9)	0.7848(5)	0.077(5)
O(1)	$^1/_3$	$^2/_3$	0.641(2)	0.040(8)
O(2)	0.194(1)	0.647(1)	0.515(1)	0.034(9)
O(3)	0.173(1)	0.765(2)	0.637(1)	0.043(10)
O(4)	0.076(1)	0.506(1)	0.638(1)	0.048(10)
O(5)	0.314(2)	0.786(1)	0.761(1)	0.06(1)
C(1)	−0.011(1)	0.615(1)	0.5626(7)	0.06(2)
C(2)	0.073	0.628	0.496	0.043(7)
C(3)	0.052	0.735	0.609	0.035(7)
C(4)	−0.031	0.504	0.611	0.052(8)
C(5)	−0.137	0.592	0.534	0.072(9)
C(6)	0.302(4)	0.844(5)	0.824(3)	0.20(2)
N(1)	1	1	0.884	0.093
C(11)	1	1	0.967	0.122
C(12)	1.007	0.888	0.860	0.130
N(2)	$^1/_3$	$^2/_3$	0.314	0.070
C(21)	0.229	0.545	0.341	0.087
C(22)	$^1/_3$	$^2/_3$	0.231	0.095
O(1w)	0.250	0.025	0.696	0.25(4)
O(2w)	1	1	0.664	0.10(3)

[a] Isotropic displacement parameters were used for N(1), N(2), and all carbon atoms except C(1).

Magnetic Measurements. Since compound **1** is air stable, no special precautions were necessary during the preparation and handling of the sample. The temperature dependence of the magnetic susceptibility of a microcrystalline sample of **1** (18.50 mg) was investigated in the range 2.2−270 K in an applied field of 1 T by using a Métronique Ingéniérie MS03 SQUID magnetometer. The contribution of the sample holder was subtracted over the whole temperature range, and diamagnetic corrections, estimated from Pascal's constants, were applied.

EHMO Calculations. Extended Hückel molecular orbital calculations based on a weighted Wolfsberg−Helmholtz formula[6] have been carried out by using the package CACAO.[7] Parameters for Fe have been taken from ref 8. For the model complex $[(H)_5FeOFe(H)_5]^{6-}$, the eclipsed, D_{4h}-symmetry conformation was chosen, with d(Fe−H) = 1.80 Å and all bond angles fixed to 90° except for the Fe−O−Fe angle, which was set equal to 180°.

(5) Sheldrick, G. M. *SHELXTL-Plus 88, structure determination software programs*; Nicolet Instrument Corp.: Madison, WI, 1988.

(6) Ammeter, J. H.; Bürgi, H.-B.; Thibeault, J. C.; Hoffmann, R. *J. Am. Chem. Soc.* **1978**, *100*, 3686.

(7) Mealli, C.; Proserpio D. M. *J. Chem. Educ.* **1990**, *67*, 399.

(8) Mukherjee, R. N.; Stack, T. D. P.; Holm, R. H. *J. Am. Chem. Soc.* **1988**, *110*, 1850.

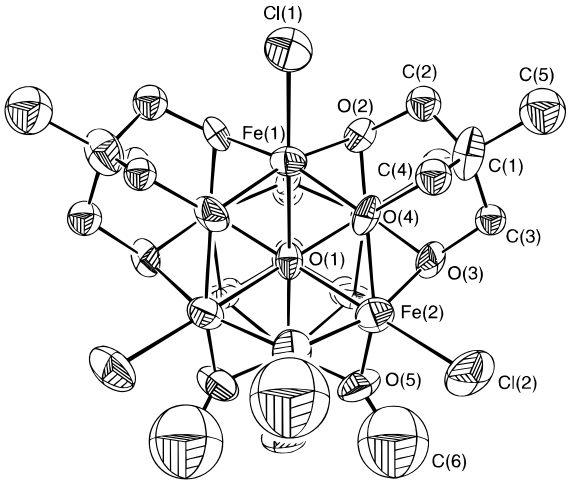

Figure 1. ORTEP drawing of $[OFe_6(H_{-3}thme)_3(OCH_3)_3Cl_6]^{2-}$. Vibrational ellipsoids are shown at the 50% probability level. Hydrogen atoms are omitted for clarity.

Table 3. Selected Bond Lengths (Å) of **1** with Esd's in Parentheses

Fe(1)···Fe(1a)	3.197(3)	Fe(1)···Fe(2)	3.208(3)
Fe(1)···Fe(2a)	3.171(3)	Fe(2)...Fe(2a)	3.178(3)
Fe(1)−Cl(1)	2.307(8)	Fe(1)−O(1)	2.27(3)
Fe(1)−O(2)	2.02(2)	Fe(1)−O(4)	1.97(2)
Fe(1)−O(2a)	1.98(2)	Fe(1)−O(3a)	1.97(2)
Fe(2)−Cl(2)	2.29(1)	Fe(2)−O(1)	2.24(3)
Fe(2)−O(3)	2.03(2)	Fe(2)−O(4)	2.06(2)
Fe(2)−O(5)	1.94(2)	Fe(2)−O(5a)	1.96(3)

Table 4. Selected Bond Angles (deg) of **1** with Esd's in Parentheses

Cl(1)−Fe(1)−O(1)	179.6(4)	Cl(1)−Fe(1)−O(2)	98.5(5)
Cl(1)−Fe(1)−O(4)	97.1(5)	Cl(1)−Fe(1)−O(2a)	97.9(5)
Cl(1)−Fe(1)−O(3a)	96.9(5)	O(1)−Fe(1)−O(2)	81.6(8)
O(1)−Fe(1)−O(4)	82.5(8)	O(1)−Fe(1)−O(2a)	82.5(8)
O(1)−Fe(1)−O(3a)	83.0(8)	O(2)−Fe(1)−O(4)	87.8(9)
O(2)−Fe(1)−O(2a)	89.8(10)	O(2)−Fe(1)−O(3a)	164.8(6)
O(4)−Fe(1)−O(2a)	165.0(6)	O(4)−Fe(1)−O(3a)	90.4(9)
O(2a)−Fe(1)−O(3a)	88.0(9)	Cl(2)−Fe(2)−O(1)	178.8(5)
Cl(2)−Fe(2)−O(3)	96.7(7)	Cl(2)−Fe(2)−O(4)	99.4(6)
Cl(2)−Fe(2)−O(5)	98.9(6)	Cl(2)−Fe(2)−O(5a)	100.9(8)
O(1)−Fe(2)−O(3)	82.4(9)	O(1)−Fe(2)−O(4)	81.3(8)
O(1)−Fe(2)−O(5)	80.3(8)	O(1)−Fe(2)−O(5a)	80.0(10)
O(3)−Fe(2)−O(4)	87.5(8)	O(3)−Fe(2)−O(5)	88.6(7)
O(3)−Fe(2)−O(5a)	161.9(10)	O(4)−Fe(2)−O(5)	161.6(8)
O(4)−Fe(2)−O(5a)	85.9(9)	O(5)−Fe(2)−O(5a)	92.4(9)
Fe(1)−O(1)−Fe(2)	90.7(1)	Fe(1)−O(1)−Fe(1a)	89.6(13)
Fe(1)−O(1)−Fe(2a)	89.3(1)	Fe(2)−O(1)−Fe(1a)	178.9(6)
Fe(2)−O(1)−Fe(2a)	90.4(13)	Fe(1)−O(2)−C(2)	116.4(9)
Fe(1b)−O(2)−C(2)	117.9(13)	Fe(1)−O(2)−Fe(1b)	106.3(9)
Fe(2)−O(3)−C(3)	116.5(10)	Fe(1b)−O(3)−C(3)	120.2(12)
Fe(2)−O(3)−Fe(1b)	105.2(11)	Fe(1)−O(4)−C(4)	120.1(13)
Fe(2)−O(4)−C(4)	114.1(14)	Fe(1)−O(4)−Fe(2)	105.5(6)
Fe(2)−O(5)−C(6)	124(3)	Fe(2a)−O(5)−C(6)	126(3)
Fe(2)−O(5)−Fe(2b)	109.2(11)		

Results and Discussion

Preparation and Structure of $[OFe_6(H_{-3}thme)_3(OCH_3)_3Cl_6]^{2-}$. The hexanuclear complex is formed almost quantitatively by the addition of 3 equiv of $[N(CH_3)_4]OH$ to an equimolar solution of $FeCl_3$ and thme in MeOH. Obviously, $[N(CH_3)_4]OH$ serves not only as base for the deprotonation of thme but also as a source for the central μ_6-oxo ligand. The structure of the complex anion is shown in Figure 1. Selected bond distances and bond angles are summarized in Tables 3 and 4, respectively. A crystallographically imposed 3-fold axis runs through the central μ_6-O atom. Although no crystallographic mirror planes are present in the space group *P*31*c*, the hexanuclear complex anion approaches C_{3v} point symmetry quite closely. The structure of the cluster core is in close agreement with that found previously for $[OFe_6(H_{-3}thme)_6]^{2-}$ (**2**) and $[OFe_6(OCH_3)_{18}]^{2-}$ (**3**).[4,9] The central μ_6-oxygen atom is octahedrally surrounded by six Fe^{III} centers. Further bridging is provided by twelve μ-alkoxo groups resulting in the "superoctahedral" $(\mu_6\text{-O})Fe_6(\mu\text{-O})_{12}$ core, having approximate O_h symmetry. The twelve alkoxo bridges originate from three methoxo and three triply deprotonated thme ligands. It is noteworthy that all the alcoholic oxygens coordinate exclusively in their deprotonated form. The six iron atoms have a distorted, octahedral coordination sphere, consisting of the μ_6-oxo ligand, four alkoxo bridges, and a terminal chloride, which is in the *trans* position to μ_6-O. Charge balance is provided by two tetramethylammonium ions, each located on a crystallographic 3-fold axis.

On the basis of the steric requirements of thme or a related tripodal polyol, there are two different possibilities for binding such a ligand to the OM_6 entity (Figure 2a): a coordination mode where all three alkoxo groups bind as μ_2-bridges (type **A**) and a mode with one terminally coordinating and two bridging alkoxo groups (type **B**). If more than one thme ligand interacts with the OM_6 unit, a variety of different arrangements have to be taken into consideration. As an example, two different structures (C_{2v} and D_{3d}) of a bis-type **A** and seven different structures ($2 \times C_1$, $2 \times C_2$, C_s, C_{2v}, C_{2h}) of the bis-type **B** coordination (Figure 2, b and c) are conceivable. There is, however, only one possible geometry for the tris-type **A** (C_{3v}), the tetrakis-type **A** (T_d), and the hexakis-type **B** (S_6) coordination. Only a few of these structures have been reported so far: the D_{3d} isomer of the bis-type **A** coordination was observed in $[OV_6\text{-}O_{12}(H_{-3}thme)_2]^{2-}$,[10] tris-type **A** coordination has been found for $[OV_6\text{-}O_6(OH)_3(H_{-3}thme)_3]^{2-}$ [11] and for $[OFe_6(H_{-3}thme)_3(OCH_3)_3Cl_6]^{2-}$ (this work), the tetrakis-type **A** structure was reported for $[OV_6\text{-}O_6(H_{-3}thmp)_4]^{2-}$ (thmp = 1,1,1-tris(hydroxymethyl)propane),[11] and the hexakis-type **B** structure has been observed for $[OFe_6(H_{-3}thme)_6]^{2-}$ (**2**).[4]

Since type **A** coordination comprises only bridging alkoxo groups, while type **B** coordination involves both bridging and terminal alkoxo groups, the ratio of deprotonated hydroxy groups per metal ion increases in going from **A** to **B**, as expressed in the following equation:

$$[Fe{-}(\mu\text{-OR}){-}Fe]^{5+} + OR^- \rightarrow 2\,[Fe{-}OR]^{2+}$$

Therefore, the coordination mode of thme can be controlled by adjusting the base to metal ratio in the preparation procedure: a low base to metal ratio leads preferentially to type **A** coordination whereas a high base to metal ratio favors type **B** coordination. This dependence of the coordination mode on the metal to base ratio is illustrated by the formation of **1** (tris-type A coordination) and **2** (hexakis-type B coordination), using 3 and 10 equiv of base/equiv of Fe, respectively.

The nonobservance of a tetrakis-type **A** structure for **1**, i.e. the coordination of only three, rather than four, thme ligands to the cluster core, is noteworthy, since thme was present in excess. Close inspection of the structural parameters (Table 5) does not indicate any obvious geometric reason for the observed absence of a fourth thme ligand. In fact, the tetrakis-type **A** structure is well-known for the above mentioned $[OV_6O_6\text{-}(H_{-3}thmp)_4]^{2-}$.[11] The formation of a tris-type **A** structure

(9) Hegetschweiler, K.; Schmalle, H. W.; Streit, H. M.; Gramlich, V.; Hund, H.-U.; Erni, I. *Inorg. Chem.* **1992**, *31*, 1299.
(10) Chen, Q.; Goshorn, D. P.; Scholes, C, P.; Tan, X.; Zubieta, J. *J. Am. Chem. Soc.* **1992**, *114*, 4667.
(11) Khan, M. I.; Chen, Q.; Höpe, H.; Parkin, S.; O'Connor, C. J.; Zubieta, J. *Inorg. Chem.* **1993**, *32*, 2929.

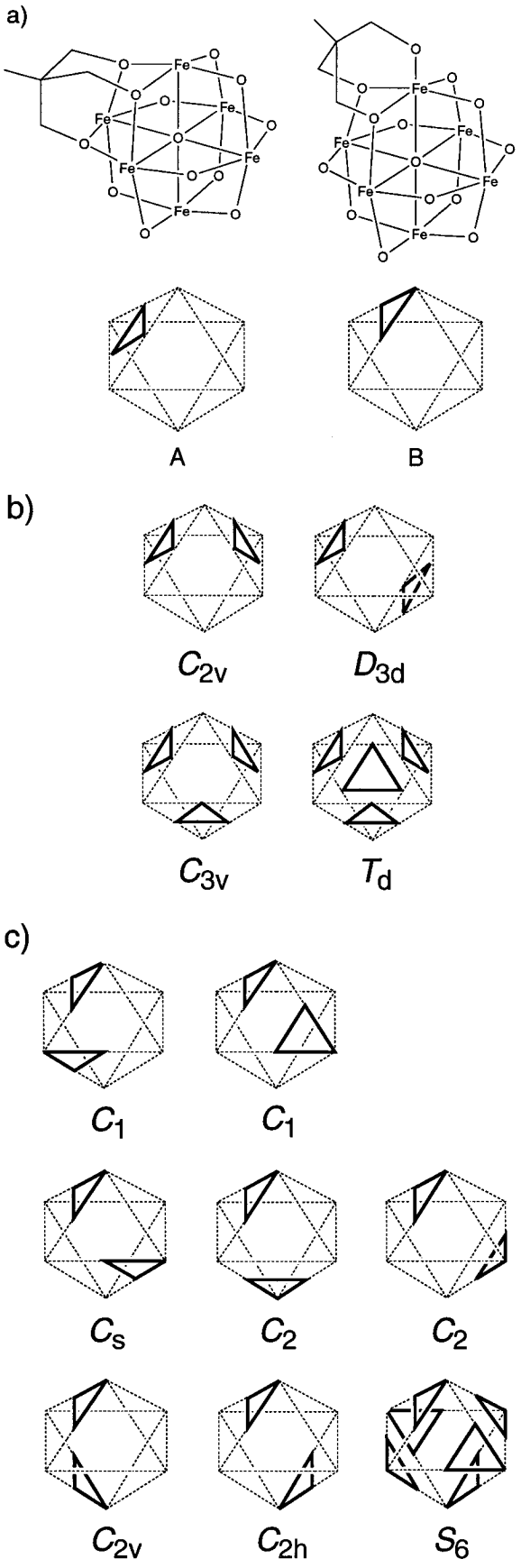

Figure 2. Possible interactions of thme with the OFe_6 unit. (a) Connectivity diagrams of the two different coordination modes (top) and the corresponding simplified representations as used in (b) and (c) (bottom). The Fe_6 octahedron is shown by dashed lines; the three coordinated oxygens of a thme ligand are indicated by a solid triangle. (b) Structures for a type **A** coordination with 2, 3, and 4 thme ligands. (c) Structures for a type **B** coordination with 2 and 6 thme ligands.

Table 5. Comparison of Characteristic Interatomic Distances (Å) and Angles (deg) in the OFe_6-O_{12} Cores of **1**−**3** (Averaged Values)

	1	**2**	**3**
Fe···Fe	3.19	3.19	3.23
μ_2-O_{thme}···μ_2-O_{thme}[a]	2.75	2.74[b]	
μ_2-O_{met}···μ_2-O_{met}	2.79		2.80[c]
Fe−μ_6-O	2.25	2.25	2.29
Fe−μ_2-O_{thme}	2.00	2.01	
Fe−μ_2-O_{met}	1.95		2.00
Fe−μ_2-O_{thme}−Fe	106.0	105.2	
Fe−μ_2-O_{met}−Fe	109.0		107.4

[a] Only intraligand distances are considered. [b] Only the distances between bridging alkoxo groups are considered. The mean intraligand O···O distance between terminal and bridging alkoxo groups is 2.84 Å. [c] Only the distances between bridging alkoxo groups are considered. The mean O···O distance between terminal and bridging methoxo ligands is 2.93 Å.

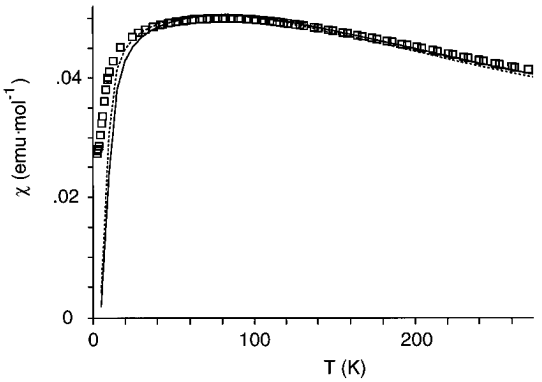

Figure 3. Temperature dependence of the molar magnetic susceptibility of compound **1** in an applied field of 1 T (squares) and calculated curves for the O_h model with $J_t = 24.2$ cm^{-1} and $J_c = 13.0$ cm^{-1} (solid line) and for the C_{3v} model with $J_t = 24.5$ cm^{-1}, $J_c = 11.5$ cm^{-1}, and $J_c' = 19.5$ cm^{-1} (dashed line).

becomes, however, understandable, if one considers that, at very high base concentration and in the absence of a tripodal polyol ligand, the corresponding $[OFe_6(OCH_3)_{18}]^{2-}$ (**3**) is formed, with the methoxo ligands occupying both the bridging and terminal positions.[9] Thus, in an alkaline solution of thme in methanol, methoxide and the tripodal tris(alkoxide) must be regarded as competing ligands. The observed tris-type **A** structure of **1** is thus a hybrid of the hypothetical $[OFe(OCH_3)_{12}Cl_6]^{2-}$ and $[OFe(H_{-3}thme)_4Cl_6]^{2-}$. The concentration of thme on the one hand and the Fe to base ratio on the other therefore represent the actual master variables which govern the number of coordinated thme ligands as well as the coordination mode of thme in such a complex.

Magnetism. The measured molar magnetic susceptibility of **1** as a function of temperature is plotted in Figure 3. The χ and $\chi \cdot T$ values at 270 K are 0.041 emu·mol^{-1} and 11.1 emu·K·mol^{-1}, respectively. The latter value is to be compared with that expected for six uncoupled $S = {}^5/_2$ spins (26.3 emu·K·mol^{-1}, assuming $g = 2.0$). On decrease of the temperature, the susceptibility slowly increases, reaching a maximum at about 90 K (0.050 emu·mol^{-1}) and then undergoes a rapid decrease. The final value at 2.2 K is 0.027 emu·mol^{-1}. The overall magnetic behavior thus indicates that essentially antiferromagnetic coupling interactions are operative between the six Fe^{III} centers.

The quantitative interpretation of the magnetic susceptibility measurements on compound **1** was carried out using a spin-only Heisenberg Hamiltonian formalism. The $Fe_6(\mu_6\text{-O})(\mu_2\text{-OR})_{12}$ core of **1** has a crystallographically imposed C_3 point-group symmetry. However, in order to reduce the number of symmetry-independent interactions, an idealized C_{3v} point-group

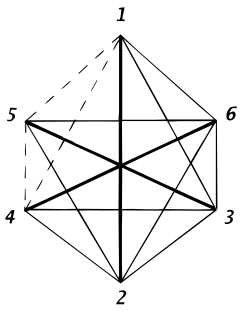

Figure 4. Topology of iron−iron magnetic exchange interactions in complex **1**. Bold lines represent *trans*-interactions, whereas dashed lines denote *cis*-interactions through μ_2-methoxo ligands.

symmetry was assumed and the 15 iron−iron magnetic-exchange interactions were described by Hamiltonian (1), with

$$\mathbf{H} = J_t(\mathbf{S}_1\cdot\mathbf{S}_2 + \mathbf{S}_3\cdot\mathbf{S}_5 + \mathbf{S}_4\cdot\mathbf{S}_6) + J_c(\mathbf{S}_1\cdot\mathbf{S}_3 + \mathbf{S}_1\cdot\mathbf{S}_6 + \mathbf{S}_2\cdot\mathbf{S}_3 + \mathbf{S}_2\cdot\mathbf{S}_4 + \mathbf{S}_2\cdot\mathbf{S}_5 + \mathbf{S}_2\cdot\mathbf{S}_6 + \mathbf{S}_3\cdot\mathbf{S}_4 + \mathbf{S}_3\cdot\mathbf{S}_6 + \mathbf{S}_5\cdot\mathbf{S}_6) + J_c'(\mathbf{S}_1\cdot\mathbf{S}_4 + \mathbf{S}_1\cdot\mathbf{S}_5 + \mathbf{S}_4\cdot\mathbf{S}_5) \quad (1)$$

$S_i = {}^5/_2$. J_t, J_c, and J_c' represent exchange-coupling constants, the subscripts *t* and *c* denote *trans*- and *cis* interactions, respectively. J_c involves μ_2-alkoxo groups from thme, whereas J_c' involves μ_2-methoxides (Figure 4).

When $J_c = J_c'$ (O_h model), Hamiltonian (1) becomes highly symmetric and leads to the energy levels in analytical form as functions of the coupling constants J_t and J_c.[12] For this reason, we first attempted to reproduce the observed magnetic behavior by setting $J_c = J_c'$. The best-fit J_t and J_c values were estimated using the Van Vleck equation[13] and standard least-squares calculations.[14] Different fitting procedures with *g* fixed to 2.0 were attempted. All of them yielded very similar results, which can be summarized as $J_t = 24.6(6)$ cm^{-1} and $J_c = 12.7(4)$ cm^{-1}.[15] The calculated best-fit curve corresponding to the experimental susceptibility ($J_t = 24.2$ and $J_c = 13.0$ cm^{-1}) is shown in Figure 3. The quality of the fit below 30 K is poor, since the calculated χ values are much lower than the experimental ones.

The condition $J_c = J_c'$ was thus relaxed, and an irreducible tensor operator approach was used to obtain the energies of the spin states.[16] Since a simultaneous fitting procedure on the parameters J_t, J_c, and J_c' would have been too time consuming, theoretical susceptibility curves for several triads of parameters were calculated. The inspection showed that an improved low-temperature fit could be obtained with $J_c < J_c'$. The calculated curve for $J_t = 24.5$ cm^{-1}, $J_c = 11.5$ cm^{-1}, and $J_c' = 19.5$ cm^{-1} is also shown in Figure 3.

The hexanuclear Fe^{III} clusters **1**−**3** yield an unprecedented opportunity of studying Fe^{III}−Fe^{III} magnetic exchange-coupling interactions through a linear oxo-bridge with an Fe−O separation of 2.25−2.26 Å. The possibility of getting accurate estimates of the exchange energies for large Fe−O distances may in fact be valuable for establishing magneto−structural correlations in polynuclear iron(III) aggregates. In this regard, our results on compound **1** are of special significance because the air stability of **1** enhances the reliability of the experimental data set.

Values of J_t as large as 25 cm^{-1} are unexpected on the basis of previous findings on a number of di- and polynuclear Fe^{III}−oxo complexes. Gorun and Lippard have recently pointed out[17] that, for several multiply-bridged Fe^{III} dinuclear units containing at least one bridging oxygen atom, an approximate inverse-exponential relationship holds empirically between the shortest superexchange pathway connecting the Fe^{III} centers ($2P$) and the corresponding coupling constant J. An analytical expression obtained by least-squares fitting through 36 experimental data points was given,[17,18] and it was concluded that, as far as the coupling constant J is concerned, electronic and steric effects are essentially reflected in the parameter P.[17] *Ab initio* calculations showed that J actually decreases as the Fe−O distance increases in the linear model compound $Na_2[Fe_2OCl_6]$.[19] However, the same dependence can be inferred even from MO calculations at the extended Hückel level. Hoffmann *et al.* have in fact shown[20] that the antiferromagnetic contributions to the exchange-coupling constant in a symmetrical d^n−d^n transition metal dimer are given approximately by

$$J_{AF} = 1/n^2 \sum_i (\Delta E_i)^2/U_i \quad (2)$$

where i runs over n pairs of MOs, each pair containing MOs which can often be roughly individuated as the *in-phase* (S) and *out-of-phase* (A) combinations of the metal d orbitals. ΔE_i is the energy separation within a given pair, and U_i accounts for interelectronic repulsion effects. According to (2), large values of J_{AF} are expected to arise from large ΔE_i separations. The energies of the MOs of the linear model complex $[(H)_5FeOFe(H)_5]^{6-}$ (D_{4h} point-group symmetry) as functions of the Fe−O separation are plotted in Figure 5. In addition to conventional symmetry labels, the members of each pair of MOs are labeled as A(d) and S(d), were d refers to the parent metal d orbital. MOs of approximate $d_{xz,yz}$ and d_{z^2} characters show the largest energy splittings. However, a dramatic reduction of the $3e_u$−$2e_g$ separation occurs as the Fe−O distance increases from 1.85 to 2.30 Å. This is to be related to the stabilization of the $3e_u$ MOs due to diminished π-antibonding interactions between the $d_{xz,yz}$ metal orbitals and the $p_{x,y}$ orbitals of the bridging oxygen. The energy of the $2e_g$ orbitals remains quite constant, since no contribution to e_g comes from the bridging ligand. On the other hand, the $4a_{1g}$−$4a_{2u}$ splitting is almost unaffected by variation of the Fe−O distance in the range examined. These two σ-type MOs of prevalent metal d_{z^2} character, with some admixture of metal p_z and s orbitals, undergo almost parallel energy changes along the reaction coordinate, reflecting essentially the synchronous decrease of the Fe(d_{z^2})−O(s) and Fe(d_{z^2})−O(p_z) overlap integrals. Replacement of hydrides with amino or hydroxide ligands as well as variation of the Fe−L_t bond distance, where L_t is the ligand

(12) Cornia, A.; Gatteschi, D.; Hegetschweiler, K. *Inorg. Chem.* **1994**, *33*, 1559.
(13) Carlin, R. L. *Magnetochemistry*; Springer: New York, 1986; p 21.
(14) E04FCF-NAG FORTRAN Library minimization routine.
(15) Minimization of $R = \sum_i[Y^{obs}_i - Y^{calc}_i]^2/\sum_i[Y^{obs}]^2$ gave $J_t = 25.0(2)$, $J_c = 12.3(1)$ cm^{-1}, and $R = 1.8 \times 10^{-4}$ for $Y = \chi\cdot T$ and $J_t = 24.2(1)$, $J_c = 13.0(1)$ cm^{-1}, and $R = 1.2 \times 10^{-4}$ for $Y = \chi$. Minimization of $R = 1/(n-p)\sum_i[(\chi^{obs}_i - \chi^{calc}_i)/\chi^{obs}_i]^2$ led to $J_t = 24.2(1)$, $J_c = 12.9(1)$ cm^{-1}, and $R = 1.2 \times 10^{-4}$. n is the number of experimental data points, and p is the number of parameters allowed to vary in the minimization routine (=2). In order to achieve convergence, when the fitting procedure was carried out on χ, the experimental data set had to be truncated below 20 K, since the model was found unable to reproduce the low-temperature behavior of the susceptibility (see ref 12).
(16) Gatteschi, D.; Pardi, L. *Gazz. Chim. Ital.* **1993**, *123*, 231. Delfs, C.; Gatteschi, D.; Pardi, L.; Sessoli, R.; Wieghardt, K.; Hanke, D. *Inorg. Chem.* **1993**, *32*, 3099.
(17) Gorun, S. M., Lippard, S. J. *Inorg. Chem.* **1991**, *30*, 1625. Turowski, P. N.; Armstrong, W. H.; Roth, M. E.; Lippard, S. J. *J. Am. Chem. Soc.* **1990**, *112*, 681.
(18) $J = 2A\exp(BP)$ with $A = 8.763 \times 10^{11}$ cm^{-1} and $B = -12.663$ Å^{-1}.
(19) Hart, J. R.; Rappé, A. K.; Gorun, S. M.; Upton, T. H. *Inorg. Chem.* **1992**, *31*, 5254.
(20) Hay, P. J.; Thibeault, J. C.; Hoffmann, R. *J. Am. Chem. Soc.* **1975**, *97*, 4884.

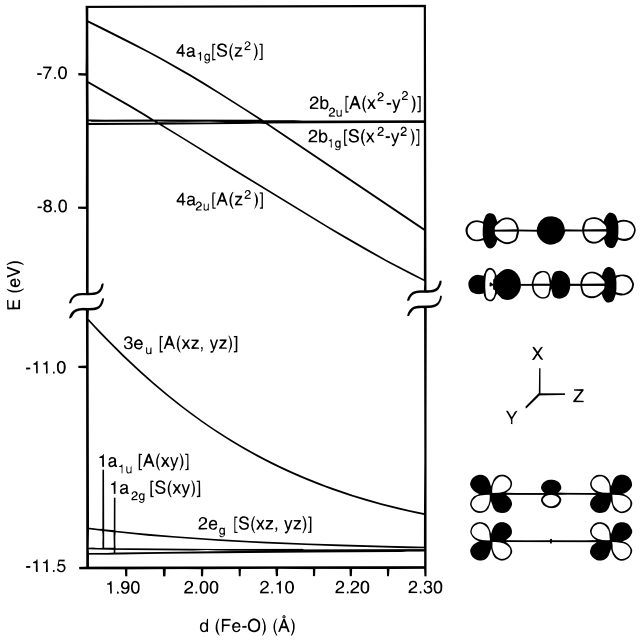

Figure 5. Walsh diagram showing the influence of the Fe−O distance on the energy of the valence MOs for the model complex $[(H)_5FeOFe(H)_5]^{6-}$. A(d)/S(d) labels (see text) are given in addition to conventional symmetry labels. Selected AO contributions to MOs are depicted for d = z^2 and *xz*, *yz*.

trans to the bridging oxygen, leads to qualitatively similar results. Inspection of Figure 5 with the aid of eq 2, therefore, suggests that, as the Fe−O separation increases, the $d_{xz,yz}$ contributions to antiferromagnetic coupling undergo a rapid decrease, perhaps with an "inverse exponential" behavior, whereas the d_{z^2} contribution is much more persistent. Indeed, a surprisingly high effectiveness of the metal-to-metal exchange pathways emerges from our estimates of the J_t constant in complexes **1**−**3**. A much smaller J_t value is predicted by the empirical inverse-exponential dependence of *J* on *P* described above ($J_t \sim 1$ cm^{-1} for $P = 2.25$ Å).[17,18] However, no Fe^{III} dinuclear fragment with $P \geq 2.10$ Å was included in the analysis by Gorun and Lippard.[18] Furthermore, all the diiron(III) units examined by the above authors have nonlinear bridging geometries and for $J \leq 24$ cm^{-1} the Fe−O−Fe angles do not exceed 106°. In iron(III)−oxo dimers with essentially constant Fe−O separations, a decrease of *J* upon bending at the bridging oxygen has been recognized and is predicted by EHMO calculations.[17,21,22] *xz*- and *yz*-type superexchange pathways are believed to play an important role in determining the observed behavior.

While *trans*-coupling is mediated by the central μ_6-oxo ligand only, *cis*-coupling can involve both the μ_6-oxo ligand and the μ_2-alkoxo bridges. A survey of available literature data[17,22,23] for similar bridging geometries shows that the latter presumably provides antiferromagnetic pathways. The shortest *cis*-superexchange pathway in **1**−**3** involves μ_2-alkoxo ligands, and if the average Fe−OR distance of 1.988 Å observed in **1** is introduced in the analytical expression given in ref 18, the value $J = 20.5$ cm^{-1} is predicted. However, the contribution of the μ_6-oxo bridge to *cis*-coupling is expected to be essentially ferromagnetic due to the Fe−(μ_6-O)−Fe *cis* angle, which is very close to 90°. Ferromagnetic exchange-coupling interactions ($J = -2.4$ cm^{-1}) have indeed been observed in an iron(III) dimer complex with phenoxy bridges and have been attributed to a remarkably acute angle at the bridging oxygen ligands (Fe−O−Fe ∼ 97°).[24]

The estimated different magnitudes of J_c and J_c' for complex **1** may reflect different efficiencies of μ_2-alkoxo ligands from thme and μ_2-methoxides in mediating magnetic-exchange interactions. Slightly shorter coupling distances (as defined in ref 17) are indeed observed through the oxygen donors from μ_2-OCH_3 ligands. Interestingly, the O_h model ($J_c = J_c'$) has been found to yield satisfactory results for complexes **2** and **3**, containing exclusively μ_2-alkoxo ligands from thme and μ_2-methoxides, respectively.

Acknowledgment. Financial support from Vifor (International) Inc., St. Gallen, Switzerland, for L.H. is gratefully acknowledged. We thank Dr. Peter Osvath, CSIRO, Clayton, Australia, for his careful reading of the manuscript.

Supporting Information Available: Listings of crystallographic data, anisotropic displacement parameters, positional parameters and *U* values of hydrogen atoms, bond lengths and bond angles (3 pages). Ordering information is given on any current masthead page.

IC960025S

(21) Tatsumi, K.; Hoffmann, R. *J. Am. Chem. Soc.* **1981**, *103*, 3328.
(22) Kurtz, D. M., Jr. *Chem. Rev.* **1990**, *90*, 585.
(23) Fallon, G. D.; Markiewicz, A.; Murray, K. S.; Quach, T. *J. Chem. Soc., Chem. Commun.* **1991**, 198. Barclay, S. J.; Riley, P. E.; Raymond, K. N. *Inorg. Chem.* **1984**, *23*, 2005. Ménage, S., Que, L., Jr. *Inorg. Chem.* **1990**, *29*, 4293.
(24) Snyder, B. S.; Patterson, G. S.; Abrahamson, A. J.; Holm, R. H. *J. Am. Chem. Soc.* **1989**, *111*, 5214.